

# Solitary and Periodic Waves in Collisionless Plasmas: The Adlam-Allen Model Revisited

J. E. Allen,<sup>1</sup> D. J. Frantzeskakis,<sup>2</sup> N. I. Karachalios,<sup>3</sup> P. G. Kevrekidis,<sup>4,1</sup> and V. Koukouloyannis<sup>3</sup>

<sup>1</sup>*Mathematical Institute, University of Oxford, Oxford, OX2 6GG, UK*

<sup>2</sup>*Department of Physics, National and Kapodistrian University of Athens, Panepistimiopolis, Zografos, Athens 15784, Greece*

<sup>3</sup>*Department of Mathematics, Laboratory of Applied Mathematics and Mathematical Modelling, University of the Aegean, Karlovassi, 83200 Samos, Greece*

<sup>4</sup>*Department of Mathematics and Statistics, University of Massachusetts, Amherst MA 01003-4515, USA*

We consider the Adlam-Allen (AA) system of partial differential equations which, arguably, is the first model that was introduced to describe solitary waves in the context of propagation of hydrodynamic disturbances in collisionless plasmas. Here, we identify the solitary waves of the model by implementing a dynamical systems approach. The latter suggests that the model also possesses periodic wave solutions –which reduce to the solitary wave in the limiting case of infinite period– as well as rational solutions which are obtained herein. In addition, employing a long-wave approximation via a relevant multiscale expansion method, we establish the asymptotic reduction of the AA system to the Korteweg-de Vries equation. Such a reduction, is not only another justification for the above solitary wave dynamics, but also may offer additional insights for the emergence of other possible plasma waves. Direct numerical simulations are performed for the study of multiple solitary waves and their pairwise interactions. The robustness of spatially periodic wave solutions is also touched upon by our numerical experiments.

## I. INTRODUCTION

The fundamental work of Adlam and Allen in 1958 and 1960 [1, 2] constituted one of the very first examples of models which may exhibit solitary wave dynamics, arguably the very first one in the important field of plasma physics. Indeed, this work preceded the hallmark efforts of Kruskal and Zabusky in 1965 [3] concerning the study of solitary waves and their interactions in the context of the famous Fermi-Pasta-Ulam problem [4] and its connections with the Korteweg-de Vries (KdV) equation [5]. In addition, the Adlam-Allen (AA) model and its solitary wave was introduced earlier than the seminal work of Washimi and Taniuti [6] who showed that the one-dimensional (1D) long-time asymptotic behavior of small-amplitude ion-acoustic waves in plasmas is described by the Korteweg-de Vries equation. The above works paved the way for numerous investigations in the nonlinear physics of plasmas, which proved to be a fertile ground for the study of solitary waves and solitons in integrable and nearly-integrable equations [7, 8]. In view of the above, the AA model seems to have received far less than its share of interest and associated research attention within the field of nonlinear waves and solitons, as has been discussed, e.g., in Ref. [9]. A recent revisiting of the relevant subject can be found in Ref. [10], where the role of the so-called  $j \times B$  force in a collisionless plasma was discussed.

Our aim in the present work is to restore this. In particular, upon shortly introducing the original motivation and formulation of the AA system of partial differential equations (PDEs), we start from its reduced –and more tractable for analysis– form presented in [2]. First we study the linear regime and show that the AA model features the linear dispersion relation of the improved Boussinesq equation, which is known to describe bidirectional shallow water waves [11]. Then, using techniques from the theory of nonlinear dynamical systems, we seek traveling waves within the model. These are identified as homoclinic connections occurring in the phase plane of a suitable conservative system, described by a second-order ordinary differential equation (ODE). The dynamical system approach enables us to identify exact and analytically expressed (as per the original efforts of [1, 2]) solitary waves in the form of homoclinic orbits. We find that these waves have speeds between once and twice the characteristic Alfvén speed [1]. This dynamical systems approach also enables the identification of periodic orbits, reminiscent of the elliptic function solutions (corresponding to the so-called “cnoidal waves”) of the KdV equation; these periodic orbits correspond to spatially periodic solutions of the original AA system. Interestingly, a degenerate case of the relevant ODE, corresponding to the case where the traveling wave propagates with the Alfvén speed, leads to the existence of a rational-type solution. Furthermore, by implementing a suitable asymptotic expansion, based on a long-wave approximation, we show that the original AA system can be approximated by the KdV equation, and that –in the small-amplitude limit– the exact solitary waves of the AA system, reduce to the KdV solitons.

The above strong justification for the potential of solitary wave dynamics motivates us to study the interaction of multiple solitary waves of the AA model, by direct numerical simulations. When colliding two such waves, we find the

interaction between them to be nearly (but not completely) elastic with a clearly observable phase shift between the two solitary waves. While our findings suggest that the AA model is likely not to be completely integrable, further investigation of the relevant topic is certainly worthwhile. We also perform a numerical study on perturbations of the identified spatially periodic solutions which suggests their potential robustness. Finally, we comment on the case of rational solutions, due to their purely mathematical interest.

The presentation of the paper is as follows: In Section II, we describe the AA model and present our analytical approaches for the identification of the exact solitary wave solutions, and the connection of the model to the KdV equation. In Section III, we present the results of our numerical studies. Section IV summarizes our findings, and briefly discusses potential future studies, for the AA and other related models.

## II. THE MODEL AND ITS ANALYTICAL CONSIDERATION

The study of [1, 2] considered electrons and ions in a plasma where the magnetic field is in the  $z$ -direction and no variations of the pertinent fields along the  $y$  or  $z$  directions are assumed as occurring. It was assumed there that appreciable amounts of energy are given to the particles in the waves (e.g., 10keV in [1]). The applications of that work were intended to be both in fusion research, as well as in the study of astrophysical phenomena such as the solar wind [12].

Let us denote by  $U_1, U_2$  the velocities along the  $x$ -direction of two distinct masses  $m_1$  and  $m_2$  and the corresponding velocities along the  $y$ -direction by  $V_1, V_2$ . We express the densities as  $n_1, n_2$  and the charges as  $e_1, e_2$ , with  $e_1 + e_2 = 0$ . Then the force balance and the Maxwell field equations lead to:

$$U_{1,t} + U_1 U_{1,x} = \frac{e_1}{m_1} \left[ E_x + \frac{V_1 B_z}{c} \right], \quad (1)$$

$$V_{1,t} + U_1 V_{1,x} = \frac{e_1}{m_1} \left[ E_y - \frac{U_1 B_z}{c} \right], \quad (2)$$

$$U_{2,t} + U_2 U_{2,x} = \frac{e_2}{m_2} \left[ E_x + \frac{V_2 B_z}{c} \right], \quad (3)$$

$$V_{2,t} + U_2 V_{2,x} = \frac{e_2}{m_2} \left[ E_y - \frac{U_2 B_z}{c} \right], \quad (4)$$

$$\frac{\partial H_z}{\partial x} = -\frac{4\pi}{c} [n_1 e_1 V_1 + n_2 e_2 V_2], \quad (5)$$

$$\frac{\partial E_y}{\partial x} = -\frac{1}{c} \frac{\partial B_z}{\partial t}, \quad (6)$$

where  $c$  denotes the speed of light. It is now assumed that the velocities along the  $x$ -direction satisfy  $U_1 = U_2$ , and similarly for the densities  $n_1 = n_2$  for the electrons and ions, thus the relative velocity between them can be referred to as  $V = V_1 - V_2$ . A key assumption here is the quasi-neutrality of the plasma. I.e., there is a very small difference between  $n_1$  and  $n_2$  responsible for the electric field, yet we approximately assume  $n_1 = n_2 \equiv n$  for practical purposes, an assumption which is valid when the electron plasma frequency is much greater than the electron gyrofrequency. The relevant criterion given in [1] also provides the condition for non-relativistic equations to be valid.

One can then switch to a Lagrangian (moving with the particles) coordinate system and adimensionalize over characteristic scales of the magnetic field  $B_*$  (i.e.,  $B \rightarrow B/B_*$ ) and density  $n_*$  (i.e.,  $n \rightarrow n/n_*$ ). In this framework, the speed is measured in units of the characteristic Alfvén speed  $V_A = \sqrt{B_*^2/(4\pi\mu n_*(m_1 + m_2))}$ , where  $\mu$  stands for the magnetic permeability of free space, while the electric field is measured in units of  $E_* = V_A B_*/c$ , i.e.,  $E \rightarrow E/E_*$ . Finally, the distances  $(x, y, z)$  are measured in units of  $d = \sqrt{m_1 m_2 c^2/(4\pi n_* \mu e_2^2 (m_1 + m_2))}$  and time is measured in units of  $t_* = (m_1 m_2)^{1/2} c/(e_2 B_*)$ , i.e.,  $t \rightarrow t/t_*$ . As a result, we obtain what we will refer to as the Adlam-Allen (AA) reduced, dimensionless PDE model:

$$R_{tt} = -\frac{1}{2}(B^2)_{xx}, \quad (7)$$

$$B_{txx} = (RB)_t. \quad (8)$$

Here,  $B$  is the rescaled (by  $B_*$ ) magnetic field, while  $R = n_*/n_{1,2}$  is the rescaled (inverse) density of ions and electrons in the field. Our intention hereafter, is to work with this reduced dimensionless version of the AA model.

### A. Derivation of exact traveling waves

The simplest nontrivial solution of the AA model (7)-(8) is expressed in the form:

$$R = R_0, \quad B = B_0, \quad (9)$$

where the constants  $R_0$  and  $B_0$  set the boundary conditions (BCs) at infinity, namely  $R \rightarrow R_0$  and  $B \rightarrow B_0$  as  $x \rightarrow \pm\infty$ . Integrating Eq. (8) over time, and using the aforementioned BCs, we can express the AA model as:

$$R_{tt} = -\frac{1}{2}(B^2)_{xx}, \quad (10)$$

$$B_{xx} = RB - R_0B_0. \quad (11)$$

It is now convenient to seek solutions of the AA model on top of the background solution,  $R = R_0$  and  $B = B_0$ , namely:

$$R(x, t) = R_0 + u(x, t), \quad B(x, t) = B_0 + w(x, t), \quad (12)$$

with the unknown fields  $u$  and  $w$  satisfying vanishing BCs at infinity, namely  $u, w \rightarrow 0$  as  $x \rightarrow \pm\infty$ . Substituting Eq. (12) into Eqs. (10)-(11), we obtain the following system of nonlinear PDEs for the fields  $u$  and  $w$ :

$$u_{tt} + B_0w_{xx} + \frac{1}{2}(w^2)_{xx} = 0, \quad (13)$$

$$w_{xx} - R_0w - B_0u - uw = 0. \quad (14)$$

Let us now consider elementary solutions of the AA model, in the form of linear waves, close to the background solution (9). To find such solutions, we assume that  $u, w \sim O(\epsilon)$ , where  $0 < \epsilon \ll 1$  is a small parameter. Then, at order  $O(\epsilon)$ , the linearization of Eqs. (13)-(14) leads to the following linear equations:

$$u_{tt} + B_0w_{xx} = 0, \quad (15)$$

$$w_{xx} - R_0w - B_0u = 0. \quad (16)$$

Obviously, using Eq. (16), one may substitute  $u = (w_{xx} - R_0w)/B_0$  into Eq. (15), and arrive at the following equation for  $w$ :

$$w_{tt} - C^2w_{xx} - \frac{1}{R_0}w_{xxt} = 0, \quad (17)$$

where

$$C^2 \equiv \frac{B_0^2}{R_0}, \quad (18)$$

is the square of the speed of small amplitude linear waves in the long-wavelength (small  $k$ ) limit; see also Eq. (19) below. Equation (17) has the form of a linearized *improved* Boussinesq equation (iBE). Generally, the Boussinesq model is known to describe the evolution of bidirectional shallow water waves [11], and the dynamics of pulses in nonlinear lattices (through a continuous approximation) [14]. A crucial difference between the standard Boussinesq equation and its iBE variant is that the latter is not prone to unphysical long-wavelength instabilities (see, e.g., Ref. [15]). The linearized iBE (17) admits plane wave solutions,  $\sim \exp[i(kx - \omega t)]$ , with the frequency  $\omega$  and wavenumber  $k$  obeying the dispersion relation:

$$\omega^2 = C^2k^2 \left(1 + \frac{k^2}{R_0}\right)^{-1}. \quad (19)$$

Considering long waves and weak dispersion, such that  $k^2/R_0 \ll 1$ , and focusing on the case of right-going waves, we may approximate the dispersion relation (19) as  $\omega \approx Ck - (C/2R_0)k^3$ , which is the dispersion relation of a Korteweg-deVries (KdV) equation. This indicates a strong connection of the AA model with the KdV equation. Indeed, below we will show that the AA model possesses exact traveling wave solutions, in the form of solitary waves, which – in the small-amplitude limit – transform into the KdV solitons.

We thus proceed by seeking solutions of the system (13)-(14) in the form of traveling waves, namely:

$$u = u(\xi), \quad w = w(\xi); \quad \xi \equiv x - vt, \quad (20)$$

where  $v$  denotes the velocity of the waves. Recalling that  $u, w \rightarrow 0$  as  $x \rightarrow \pm\infty$ , Eq. (13) can readily be integrated twice with respect to  $\xi$ , leading to:

$$u = -\frac{1}{v^2} \left( B_0 w + \frac{1}{2} w^2 \right). \quad (21)$$

Substituting Eq. (21) into Eq. (14), we obtain the following nonlinear ODE for the field  $w$ :

$$w'' = \frac{B_0^2}{v^2 C^2} (v^2 - C^2) w - \frac{3B_0}{2v^2} w^2 - \frac{1}{2v^2} w^3, \quad (22)$$

where the primes denote differentiation with respect to  $\xi$ . Equation (22) can be viewed as an equation of motion of a particle in the presence of the effective potential  $V(w)$  given by:

$$V(w) = -\frac{B_0^2}{2v^2 C^2} (v^2 - C^2) w^2 + \frac{B_0}{2v^2} w^3 + \frac{1}{8v^2} w^4. \quad (23)$$

The total energy of the system is

$$E(w, w') = \frac{1}{2} w'^2 + V(w) = E_0, \quad (24)$$

where the constant of integration  $E_0$  represents the total initial energy of the effective oscillator which is conserved along its motion.

A simple analysis shows that if  $v < C$ , then there exists a sole fixed point at  $w = 0$  being stable center, at which the potential  $V$  attains its global minimum. As a result, all solutions of Eq. (22) are periodic and can, in principle, be expressed in terms of the Jacobi elliptic functions.

On the other hand, if  $v > C$  there exist for  $w \geq 0$ , two fixed points: an unstable saddle point at  $w = 0$  (corresponding to the global maximum of the potential  $V$  for  $w \geq 0$ ), and a stable center at  $w = 8(v/C - 1)B_0$  (corresponding to the global minimum of  $V$  for  $w \geq 0$ ). The graph of the potential  $V(w)$  (23) in this case, is portrayed in the top-left panel of Figure 1. This is a case of particular interest, since, there exists a homoclinic orbit (separatrix), namely a trajectory of infinite period, which corresponds to a solution decaying at infinity, i.e., a solitary wave. The top-right panel of Figure 1 depicts orbits of the dynamical system (22) corresponding to various energy values (straight horizontal lines shown in the graph of the potential  $V(w)$ , depicted in the top left-panel). The homoclinic orbit [continuous (red) curve forming a “loop” as shown in the top-right panel] corresponds to the energy  $E_0 = V(0) = 0$  [the continuous (red) horizontal line shown in the top-left panel]. The closed orbits [dashed (blue) curves] correspond to energy values  $E_0 < 0$ , and are associated with spatially periodic solutions. We will discuss them in Section III C.

Let us focus on the homoclinic orbit. In order to derive the corresponding solution, we use the first integral Eq. (24) for the value  $E_0 = 0$ , which is the energy of the homoclinic solution. Then, a second integration, i.e.,  $\int dw / \sqrt{-2V(w)} = \xi - x_0$  ( $x_0$  is a constant), leads to the implicit form of the solution, which eventually can be expressed in the following explicit form:

$$w(x, t) = \frac{2B_0}{C} (v^2 - C^2) \frac{1}{C + v \cosh(\theta)}, \quad (25)$$

$$\theta \equiv \frac{B_0}{vC} \sqrt{v^2 - C^2} (x - vt - x_0). \quad (26)$$

In Eq. (26), the constant  $x_0$  represents the initial position of the solitary wave. Notice that due to the aforementioned necessary condition,  $v > C$ , for the existence of the solitary wave (25), it turns out that this exact traveling wave solution is in fact traveling with a speed larger than that of the long-wavelength linear waves. On the other hand, the positive density constraint of  $R > 0$ , by using (12)-(21)-(25), yields also an upper bound for the speed, namely  $v < 2C$ . Thus, in terms of the velocity  $v$ , the domain of existence of a physically relevant solitary wave is:

$$C < v < 2C. \quad (27)$$

Summarizing our findings presented in this section, we have derived an exact, exponentially localized, travelling wave solution of the AA model, of the form:

$$R(x, t) = R_0 - \frac{1}{v^2} w(x, t) \left[ B_0 + \frac{1}{2} w(x, t) \right] := R^s(x, t), \quad (28)$$

$$B(x, t) = B_0 + w(x, t) := B^s(x, t), \quad (29)$$

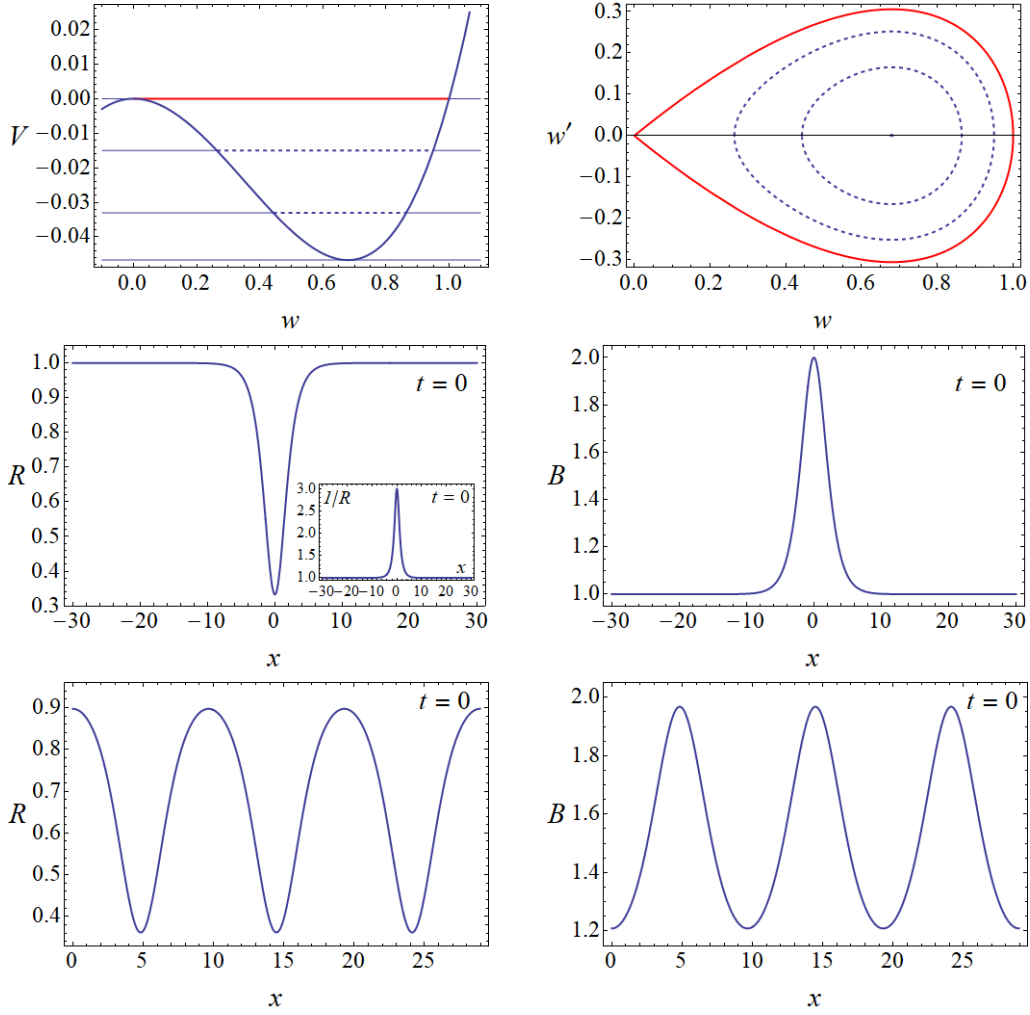


FIG. 1: (Color online) Top row: the left panel shows the graph of the effective potential  $V(w)$  (23), with some typical energy values depicted by the straight horizontal lines. Parameter values:  $B_0 = R_0 = 1$ ,  $v = 1.5$ . The continuous (red) line corresponds to the energy  $E_0 = V(0) = 0$  which is the value of the energy for the homoclinic orbit. The dashed lines depict energy values  $E_0 < 0$ , which correspond to closed, periodic orbits. The right panel shows orbits in the  $(w, w')$  phase-plane of (22), corresponding to the energy values of the top-left panel. The continuous (red) curve depicts the homoclinic orbit corresponding to the energy  $E_0 = V(0) = 0$ . The dashed closed curves are associated with the periodic solutions corresponding to energy values  $E_0 < 0$ . Middle row: The middle-left panel shows the profile of the solitary wave for  $R$  given by (28), at  $t = 0$ . We also show the quantity  $1/R$  as an inset, as the latter physically represents the density of the charged particles. The middle-right panel shows the profile of the soliton solution for  $B$  given by (29), at  $t = 0$ . Bottom row: A spatially periodic solution corresponding to the energy  $E_0 = -0.015$ . The left panel depicts the profile of the  $R^p$  periodic component of the solution, at  $t = 0$ , while the right panel depicts the profile of its  $B^p$  periodic component, at  $t = 0$ .

with  $w(x, t)$  given by Eqns. (25)-(26). This is the same wave as identified in the original [1] work, yet the approach used herein will enable us to obtain a considerably wider family of solutions in what follows. The profiles of these solutions at  $t = 0$  are depicted in the middle row of Figure 1. The middle-left panel of Figure 1 shows the profile of  $R^s(x, 0)$  and the middle-right panel of Figure 1 shows the profile of  $B^s(x, 0)$  corresponding to a pulse on top of the finite background  $B_0 = 1$ . The inset of the left panel shows  $1/R$  which is proportional to the particle density.

### B. Connection to the KdV equation

The derivation of the linearized improved Boussinesq equation (17) that describes the linear properties of the model, as discussed in Section II A, suggests the possibility of establishing an asymptotic connection between the AA system

and the KdV equation. To do this, it is convenient to employ the so-called long-wave approximation [16], and introduce the slow variables:

$$X = \epsilon^{1/2}(x - Ct), \quad T = \epsilon^{3/2}t, \quad (30)$$

where  $0 < \epsilon \ll 1$  is a formal small parameter. Using these variables, Eqs. (13)-(14) are respectively expressed as follows:

$$\begin{aligned} & \epsilon \left( C^2 - \frac{B_0^2}{R_0} \right) w_{XX} - \epsilon \frac{1}{R_0} \partial_X^2 \left( \frac{1}{2} B_0 w^2 - C^2 uw \right) \\ & - \epsilon^2 \left( 2Cw_{XT} - \frac{C^2}{R_0} w_{XXX} \right) = O(\epsilon^j), \quad j \geq 3, \end{aligned} \quad (31)$$

$$\epsilon w_{XX} - R_0 w - B_0 u - uw = 0. \quad (32)$$

It can now readily be observed that the first term in the right-hand side of Eq. (31) vanishes – see Eq. (18). Furthermore, upon introducing the following perturbation expansions of the fields  $u$  and  $w$  with respect to  $\epsilon$ :

$$u = \epsilon u_1 + \epsilon^2 u_2 + \dots, \quad w = \epsilon w_1 + \epsilon^2 w_2 + \dots, \quad (33)$$

we can obtain from Eqs. (31)-(32) the following results. First, at order  $O(\epsilon)$ , we derive from Eq. (32) the following equation connecting the unknown fields  $u_1$  and  $w_1$ :

$$u_1 = -\frac{R_0}{B_0} w_1. \quad (34)$$

Next, using Eq. (34), the nonlinear contribution [second term in Eq. (32)] arising at  $O(\epsilon^3)$  in Eq. (32) becomes  $-(3B_0/R_0)(w_1 w_{1X})_X$ . As a result, at  $O(\epsilon^3)$ , integration of Eq. (32) over  $X$  leads to the following KdV equation:

$$2Cw_{1T} + \frac{C^2}{R_0} w_{1XXX} + \frac{3B_0}{R_0} w_1 w_{1X} = 0. \quad (35)$$

It is well known that the KdV equation is a completely integrable system possessing soliton solutions (see, e.g., Ref. [11]). In particular, the single soliton solution of Eq. (35), when expressed in terms of the original variables  $x$  and  $t$ , gives rise to the following approximate solution [valid up to order  $O(\epsilon)$ ] of the system (13)-(14):

$$w(x, t) = \epsilon \kappa^2 \frac{4B_0}{R_0} \text{sech}^2(\eta), \quad (36)$$

$$u(x, t) = -4\epsilon \kappa^2 \text{sech}^2(\eta), \quad (37)$$

$$\eta \equiv \epsilon^{1/2} \kappa \left[ x - C \left( 1 + \epsilon \kappa^2 \frac{2}{R_0} \right) t - x_0 \right], \quad (38)$$

where  $\kappa$  is an arbitrary  $O(1)$  parameter characterizing the amplitude, the width and the velocity of the KdV soliton. Thus, the original AA system (7)-(8) supports the following approximate solution:

$$R(x, t) \approx R_0 \left[ 1 - \epsilon \frac{4\kappa^2}{R_0} \text{sech}^2(\eta) \right], \quad (39)$$

$$B(x, t) \approx B_0 \left[ 1 + \epsilon \frac{4\kappa^2}{R_0} \text{sech}^2(\eta) \right]. \quad (40)$$

We will now show that in the limit of  $v \rightarrow C$ , the solitary wave (25) becomes the KdV soliton (36). To do this, we use  $v \approx C$ , and approximate  $v^2 - C^2$  as follows:  $v^2 - C^2 = (v + C)(v - C) \approx 2C(v - C)$ . Then, using the identity  $1 + \cosh(\theta) = 2 \cosh^2(\theta/2)$ , we may rewrite Eq. (25) in the form:

$$w(x, t) = \frac{2B_0}{C} (v - C) \text{sech}^2 \left[ \frac{B_0}{2vC} \sqrt{v^2 - C^2} (x - vt - x_0) \right]. \quad (41)$$

It is now evident that much like the KdV soliton, the amplitude and width of the solitary wave (41) are set by a single parameter, namely  $v - C$ . The limit  $v \rightarrow C$  is, in fact equivalent with the small amplitude limit, whereby  $v - C$  plays

now the role of a small parameter. Then, employing the small parameter  $\epsilon$ , and noticing that  $\kappa^2(4B_0/R_0) = O(1)$  as per our analysis, we can set

$$v - C = \epsilon \kappa^2 C(2/R_0). \quad (42)$$

This automatically implies that the amplitudes of the solitary wave (41) and the KdV soliton (36) are equal. Furthermore, it can readily be observed that the velocity of the solitary wave (41) becomes

$$v = C[1 + \epsilon \kappa^2(2/R_0)],$$

which is equal to the velocity of the KdV soliton (36). Finally, the inverse width of the solitary wave (41) reads:

$$\frac{B_0}{2vC} \sqrt{v^2 - C^2} \approx \frac{B_0}{2vC} \sqrt{2C(v - C)} = \frac{B_0}{2vC} \sqrt{2C^2 \epsilon \kappa^2(2/R_0)} = \epsilon^{1/2} \kappa,$$

where we have used the definition of the velocity  $C$  in Eq. (18). Thus, the inverse width of the solitary wave (41) becomes equal to the one of the KdV soliton (36).

Concluding this section, we have shown that in the limit  $v \rightarrow C$ , i.e., in the small-amplitude limit, the solitary wave (41) transforms into the KdV soliton (36), which further highlights the asymptotic connection of the AA model with the KdV equation.

### C. A rational solution

As it was shown in Section II A, the AA system supports the exact, exponentially localized, solitary wave solutions (28)-(29). Nevertheless, the system also possess still another exact, but weakly localized, solitary wave solution, which features an algebraic decay as the travelling wave coordinate  $\xi \rightarrow \pm\infty$ . This solution exists in the limiting case case where  $v = C$ . Indeed, in this case, the ODE (22) reduces to the form:

$$w'' = -\frac{3B_0}{2v^2} w^2 - \frac{1}{2v^2} w^3, \quad (43)$$

where, now, the fixed point  $w = 0$  becomes an *inflection point* for the potential  $V(w)$ . In such a situation, it is possible to identify an exact, algebraically decaying, solution of Eq. (43), of the following form:

$$w(x, t) = -\frac{4B_0}{1 + R_0 \xi^2}, \quad \xi = x - Ct. \quad (44)$$

This rational waveform, gives rise to the following exact solution of the original AA model (7)-(8):

$$R(x, t) = R_0 \left[ 1 - 4 \frac{1 - n_0 \xi^2}{(1 + R_0 \xi^2)^2} \right] := R^r(x, t), \quad (45)$$

$$B(x, t) = B_0 \left( 1 - \frac{4}{1 + R_0 \xi^2} \right) := B^r(x, t). \quad (46)$$

This solution, although interesting in its own right from a mathematical point of view, suggests an unphysical situation, namely a negative (inverse) density as it is clear from (46).

## III. NUMERICAL INVESTIGATIONS

In this section, we perform numerical simulations, aiming to investigate the dynamics of the solitary and periodic waves identified in the previous sections. First, we explore the dynamics of the single exact solitary wave when considered as an initial condition for the system. Second, we explore the dynamics of two solitary waveforms and their potential interaction dynamics. Third, we proceed to a numerical study examining the robustness of periodic solutions in the presence of Fourier mode perturbations. Finally, due to their mathematical interest (as they are not physically relevant in the context of the AA model), we briefly comment on the rational solutions.

The numerical integration is performed for the following initial-boundary value problem of the AA system (7)-(8), with initial conditions

$$R(x, 0) = \varrho_0(x), \quad n_t(x, 0) = \varrho_1(x), \quad B(x, 0) = \beta_0(x), \quad (47)$$

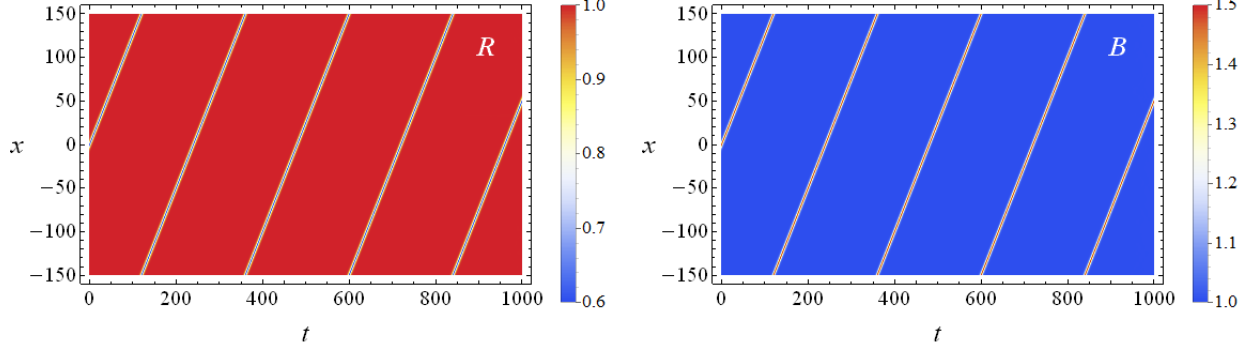


FIG. 2: (Color online) Contour plots of the spatiotemporal evolution of the solitary wave initial conditions ( $R^s(x, 0), B^s(x, 0)$ ). Left panel: Evolution of the  $R$ -component of the solution. Right panel: Same as the left panel, but for the  $B$ -component of the solution. Parameter values: velocity  $v = 1.5$ ,  $B_0 = R_0 = 1$  ( $C = 1$ ),  $L = 150$ .

and periodic boundary conditions on the interval  $[-L, L]$ , for  $B$  and its first derivative  $B_x$ ,

$$B(-L, t) = B(L, t), \quad B_x(-L, t) = B_x(L, t). \quad (48)$$

The initial-boundary value problem (7)-(8)-(47)-(48) is integrated numerically by implementation of the method of lines [17]; a tensor product grid discretization scheme is considered for the spatial integration, while, for the integration with respect to time a 4th - 5th-order adaptive-step Runge-Kutta method is used.

### A. Dynamics of the single-soliton solutions

Numerical integration of the system (7)-(8)-(47)-(48) using as initial conditions the analytical solutions (28) and (29) at  $t = 0$ , i.e.,  $\varrho_0(x) = R^s(x, 0)$ ,  $\varrho_1(x) = R_t^s(x, 0)$ ,  $\beta_0(x) = B^s(x, 0)$ , verified the stability of their time propagation (and as a by-product, the accuracy of the numerical method). Their spatiotemporal evolution is depicted in the contour plots of Figure 2. The left panel portrays the dynamics of the  $R$ -component of the numerical solution, while the right panel the dynamics of the  $B$ -component of the same solution. The system is integrated for  $L = 150$  and for this choice the initial error at the boundaries is far smaller than the accuracy used in the calculations. The parameter values are  $B_0 = 1$ ,  $R_0 = 1$ ,  $x_0 = 0$ , while the velocity is  $v = 1.5 > C = 1$ , as  $C$  is defined by (18). The initial data evolve as the exact soliton solutions (28) and (29), preserving their initial profile and speed.

### B. Interaction dynamics of two solitons

The second numerical experiment investigates the dynamics of two solitary waveforms, initialized by a superposition of the analytically derived soliton solutions presented in Section II A, i.e., (28) and (29). More precisely, we shall consider the dynamics of initial conditions of the form:

$$R(x, 0) = R_0 - \frac{1}{v_1^2} w_1(x, 0) \left[ B_0 + \frac{1}{2} w_1(x, 0) \right] - \frac{1}{v_2^2} w_2(x, 0) \left[ B_0 + \frac{1}{2} w_2(x, 0) \right] := R^{ds}(x, 0), \quad (49)$$

$$B(x, 0) = B_0 + w_1(x, 0) + w_2(x, 0) := B^{ds}(x, 0), \quad (50)$$

with  $w_i(x, t) = w(x, t)|_{(x_0=x_i, v=v_i)}$ ,  $i = 1, 2$ , and  $w(x, t)$  given by Eq. (25).

The expressions (49)-(50) describe the interaction between two solitons defined by the analytical solutions (28) and (29), with velocities  $v_1$  and  $v_2$ , respectively. Let us recall that the permitted and physically relevant velocities should be such that  $v_i \in (C, 2C] = (v_{\min}, v_{\max}]$ .

*a. Soliton collision: two-soliton velocities  $v_1 = 1.8$  and  $v_2 = 1.2$ .* We assume that the parameter values are  $B_0 = 1$ ,  $R_0 = 1$ . Then  $C = 1$ . First, we examine the case where the velocity of the first soliton  $v_1 = 1.8$  is close to the upper boundary point  $v_{\max} = 2$  of the permitted interval  $(1, 2)$ , and the velocity of the second soliton  $v_2 = 1.2$  is close to the lower boundary point  $v_{\min} = 1$ . The system (7)-(8)-(47)-(48) is integrated for the initial conditions  $\varrho_0(x) = R^{ds}(x, 0)$ ,  $\varrho_1(x) = R_t^{ds}(x, 0)$ ,  $\beta_0(x) = B^{ds}(x, 0)$ , for the above velocities  $v_1$  and  $v_2$ . The first soliton is



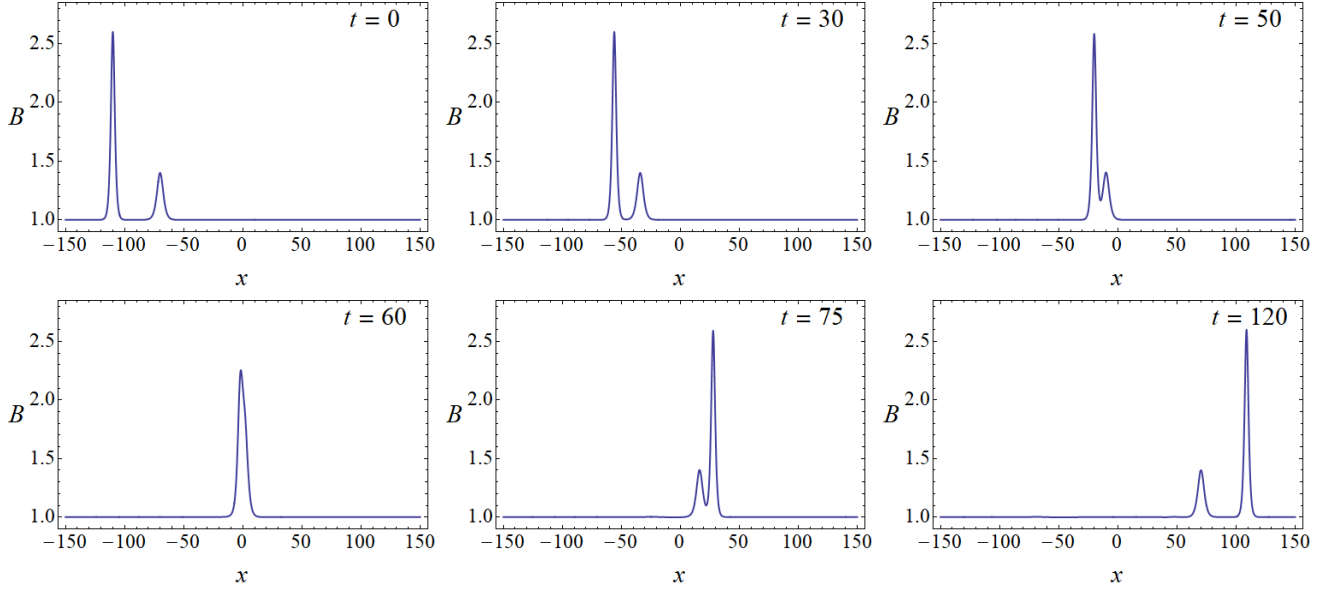


FIG. 3: (Color online) Snapshots of the evolution of the two solitary waves initial condition  $(R^{ds}(x, 0), B^{ds}(x, 0))$ , with velocities  $v_1 = 1.8$  and  $v_2 = 1.2$ . In the frames, the  $B$ -component of the solution is depicted. The initial positions of the waves are  $x_1 = -110$  (and velocity  $v_1 = 1.8$ ),  $x_2 = -70$  (and velocity  $v_2 = 1.2$ ). Parameter values:  $B_0 = 1$ ,  $R_0 = 1$  and  $L = 150$ .

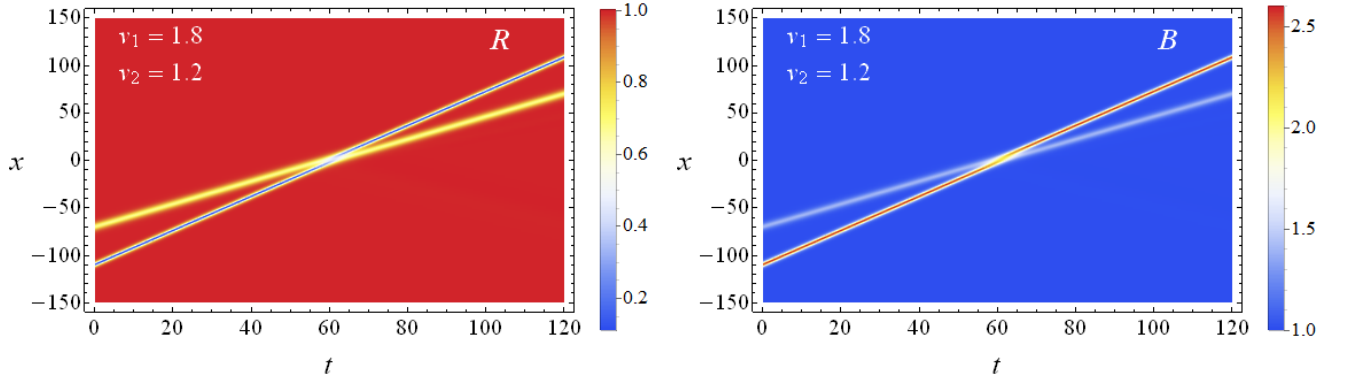


FIG. 4: (Color online) Contour plots of the spatiotemporal evolution of the two-soliton initial conditions  $(R^{ds}(x, 0), B^{ds}(x, 0))$ , for the velocities  $v_1 = 1.8$  and  $v_2 = 1.2$ . The rest of parameters are fixed as in Fig. 3. Left panel: The  $R$ -component of the solution is shown. Right panel: Same as before but for the  $B$ -component.

initially positioned at  $x_1 = -110$  and the second soliton at  $x_2 = -70$ . We ensured in this way that the waves were well separated and in adequate distance from the boundaries in order not to introduce any numerical artifacts. The system is integrated for  $t \in [0, 200]$  and  $L = 150$ , which is a sufficient setting for the study of the interaction dynamics of the two solitons which is our main goal.

Figure 3 presents snapshots of the evolution of the  $B$ -component of the described two-wave initial condition (49)-(50), for  $t \in [0, 120]$ . The snapshots justify the collision of the two solitons and the near preservation (see the discussion below) of their initial profiles and velocities after their collision; the faster and taller soliton of velocity  $v_1 = 1.8$  catches up with the slower and shorter soliton and eventually overtakes it. The collision is alternatively visualized by the contour plots of the dynamics of the two-soliton initial conditions  $R^{ds}(x, 0)$  and  $B^{ds}(x, 0)$ , depicted in Figure 4. The left panel depicts the evolution of the  $R$ -component of the numerical solution, while the right panel depicts the corresponding  $B$ -component.

An important finding is that the collision of the two solitons is nearly –but not genuinely– elastic. This fact suggests the non-integrability of the system (7)-(8). This can be seen in Figure 5, depicting snapshots of the dynamics of the  $B$ -component of the solution at  $t = 85$  (left panel) and  $t = 135$  (right panel), respectively, for the two solitary wave

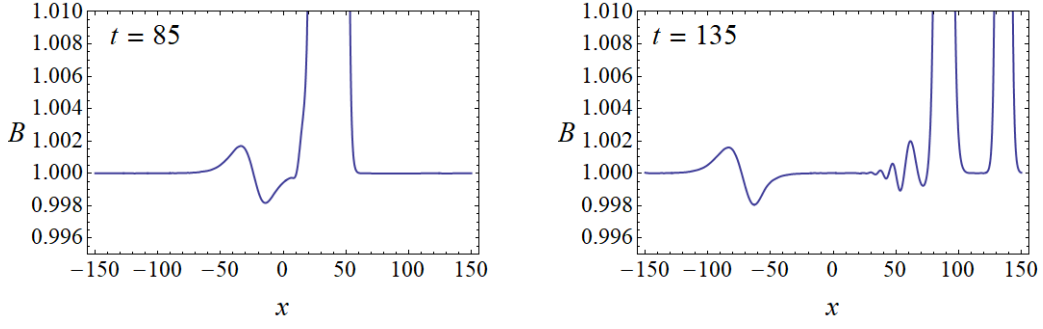


FIG. 5: (Color online) Snapshots of the evolution of the two solitary wave initial condition  $(R^{ds}(x,0), B^{ds}(x,0))$ , with velocities  $v_1 = 1.8$  and  $v_2 = 1.2$ . A magnification around the tail during and after the collision of the solitons, of the  $B$ -component of the solution is shown. The rest of parameters are fixed as in Fig. 3.

initial conditions. The snapshots offer a magnified view around the tail of the solution, during and after the collision of the two waves. In both snapshots, we observe the emission of small amplitude wavepackets.

*b. Repulsive interaction: two-soliton velocities  $v_1 = 1.9$ ,  $v_2 = 1.8$ .* We consider again the parameter values  $B_0 = 1$ ,  $R_0 = 1$ . Now, we will examine the dynamics of two waves initialized through  $R^{ds}(x,0)$  and  $B^{ds}(x,0)$ , with velocities close to each other, but also being close to the upper boundary point  $v_{\max} = 2$  of the permitted interval  $(1, 2]$ . For instance, we will consider the values  $v_1 = 1.9$  and  $v_2 = 1.8$ . The system is integrated for  $t \in [0, 600]$  and  $L = 150$ . In this case, since the relative velocity of the two solitons is smaller, a larger time interval is required in order to study the corresponding interaction dynamics.

Figure 6 presents snapshots of the evolution of the two wave initial condition  $(R^{ds}(x,0), B^{ds}(x,0))$ . In the panels, the  $B$ -component of the solution is depicted. In this case, we observe an interaction of repulsive type: the two

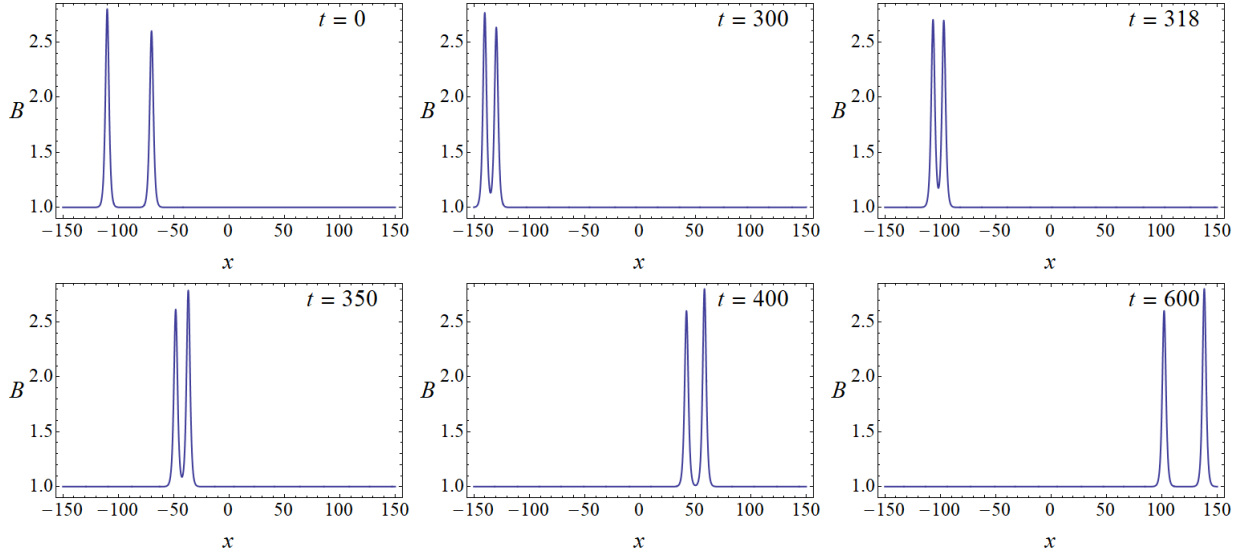


FIG. 6: (Color online) Snapshots of the evolution of the two-soliton initial condition  $(R^{ds}(x,0), B^{ds}(x,0))$ , with velocities  $v_1 = 1.9$  and  $v_2 = 1.8$ . The  $B$ -component of the solution is depicted. Initial positions of the solitons  $x_1 = -110$  (soliton with velocity  $v_1 = 1.9$ ),  $x_2 = -70$  (soliton with velocity  $v_2 = 1.8$ ). Parameter values:  $B_0 = 1$ ,  $R_0 = 1$  and  $L = 150$ .

coherent structures exchange their velocities, and afterwards, they continue their motion in the same direction. This interaction is also illustrated in the contour plots of Figure 7 (left panel for the dynamics of  $R$ -component and right panel for the corresponding dynamics of  $B$ -component of the solution).

In this case, the emission of small amplitude waves is weaker if compared with the one of the previous example for the velocities  $v_1 = 1.8$  and  $v_2 = 1.2$  (where we observed the collision). The evidence is shown in Figure 8, presenting snapshots of the evolution of the  $B$ -component of the solution, with a magnified view around its tail; the emerging wavepackets are weak yet discernible in the snapshot for  $t = 430$  (right panel). Effectively, it can be observed here that the weak relative kinetic energy of the structures is not sufficient to overcome the potential energy barrier of the

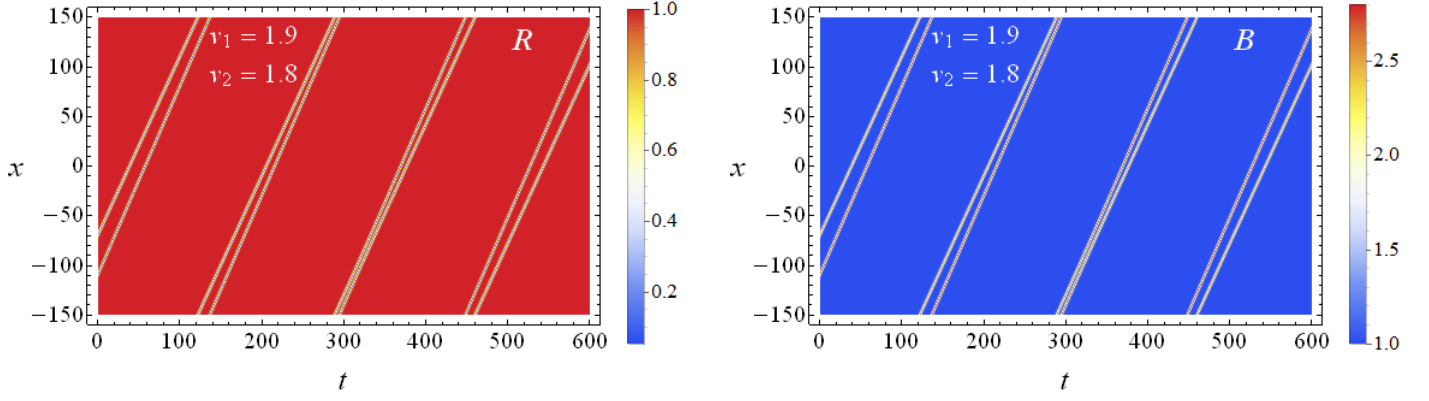


FIG. 7: (Color online) Contour plots of the spatiotemporal evolution of the two solitary wave initial conditions ( $R^{ds}(x,0)$ ,  $B^{ds}(x,0)$ ), for  $v_1 = 1.9$  and  $v_2 = 1.8$ . The rest of parameter values are fixed as in Fig. 6. Left panel: The  $R$ -component of the solution is shown. Right panel: The same as before but for the  $B$ -component.

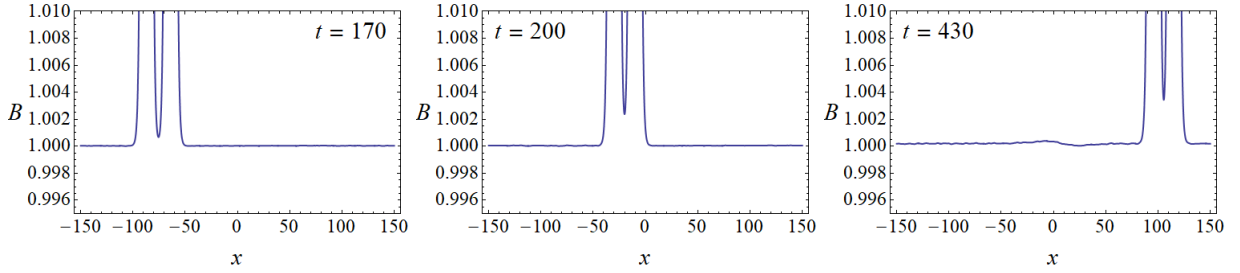


FIG. 8: Snapshots of the evolution of the two wave initial condition ( $R^{ds}(x,0)$ ,  $B^{ds}(x,0)$ ), with velocities  $v_1 = 1.9$  and  $v_2 = 1.8$ . A magnification around the tail, during the repulsive interaction of the solitons, of the  $B$ -component of the solution is shown. The rest of parameter values are fixed as in Fig. 6.

waves' repulsive interaction. As a result, a minimal dispersive wake is only emitted in the process.

### C. Periodic Solutions

As was analyzed in Section II A, and visualized in Figure 1, for energy values  $E_0 < 0$ , we detect spatially periodic, traveling wave solutions, associated with the closed curves inside the homoclinic loop of the  $(w, w')$  phase-plane. Let us recall that the bottom row of Figure 1 shows the profiles of the  $R^p(x, t)$ -component (left panel), and of the  $B^p(x, t)$ -component (right panel) at  $t = 0$ , for such a spatially periodic solution (as denoted by the superscript  $p$ ), corresponding to the energy  $E_0 = -0.015$ . We investigated numerically the stability of these spatially periodic solutions in the presence of small amplitude, Fourier mode perturbations, considered as initial conditions of the dimensionless problem. Instead of the symmetric interval  $[-L, L]$ , the periodic boundary conditions (48) are implemented on the interval  $[0, m\lambda]$ , where  $\lambda$  stands for the wavelength of the solution. The wavelength  $\lambda$  can be calculated for a given set of parameters, by integration of Eq. (24). In all of the examples considered herein, we assumed  $B_0 = R_0 = 1$ , and  $v = 1.5$ . The results are shown for  $t \in [0, 200]$ , for the sake of clarity of the presented graphics; however, we confirmed that the relevant solutions persist for at least twice the time horizon shown.

In Figure 9, the spatiotemporal evolution of a perturbed spatially periodic initial condition, is shown. The unperturbed initial condition ( $R^p(x, 0), B^p(x, 0)$ ) explored is the one with energy  $E_0 = -0.03$  where we have considered  $m = 5$ . In this condition we perturb the component  $B$ -component by adding a Fourier mode and the initial condition becomes  $(R^p(x, 0), B^p(x, 0) + 0.01 \sin(3Kx))$ , where  $K = 2\pi/\lambda$  denotes the wavenumber associated with the wavelength  $\lambda$  of the solution. Moreover, Figure 10 depicts the dynamics of another perturbed spatially periodic initial condition of the form  $(R^p(x, 0) + 0.01 \sin(10Kx), B^p(x, 0))$  for the case example of an  $m = 3$ . The unperturbed initial condition corresponds to energy  $E_0 = -0.01$ .

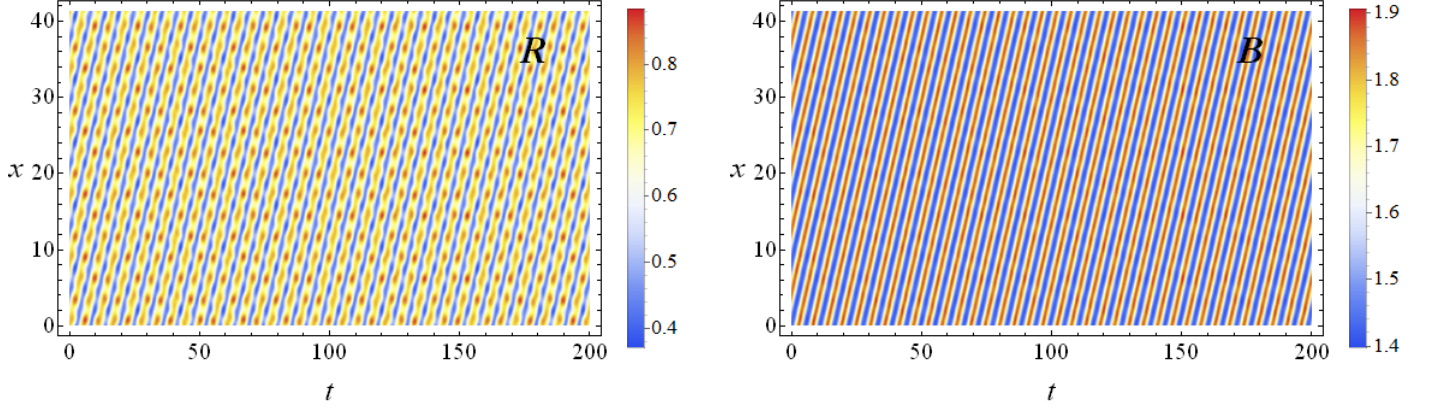


FIG. 9: (Color online) Contour plot of the spatiotemporal evolution of the perturbed spatially periodic solution  $(R^p(x, 0), B^p(x, 0) + 0.01 \sin(3Kx))$ . Left panel: The  $R$ -component of the solution. Right panel: The  $B$ -component of the solution. Parameter values:  $B_0 = R_0 = 1$ ,  $v = 1.5$ . The spatial interval is  $[0, m\lambda]$  with  $m = 5$ ;  $\lambda$  is the spatial period of the solution and  $K = 2\pi/\lambda$  is the wavenumber associated with the wavelength  $\lambda$ . The energy associated with the unperturbed initial conditions is  $E_0 = -0.03$ .

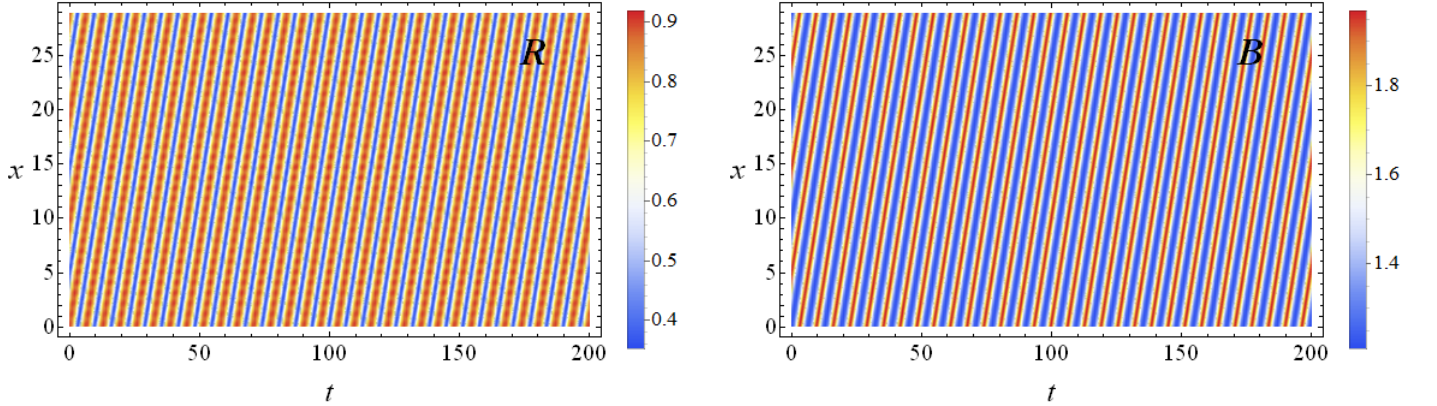


FIG. 10: (Color online) Contour plot of the spatiotemporal evolution of the perturbed spatially periodic solution  $R^p(x, 0) + 0.01 \sin(10Kx), B^p(x, 0)$  with  $m = 3$ . Left panel: The  $R$ -component of the solution. Right panel: The  $B$ -component of the solution. Parameter values:  $B_0 = R_0 = 1$ ,  $v = 1.5$ . Energy of the unperturbed initial conditions  $E_0 = -0.01$ .

In both of the above examples, the evolution of the perturbed spatially periodic initial condition appears to robustly preserve the relevant waveform without giving rise to any growth modes, suggesting its dynamical stability. This is in line with what has been found in the case of cnoidal waves in the KdV equation; see, e.g., the work of [20].

#### D. Rational Solution

As was shown in Section II C, the case  $v = C$  gives rise to a degenerate scenario for the dynamical system (43). The top-left panel of Figure 11 shows the graph of the effective potential in this case: the potential  $V$  has an inflection point at  $w = 0$ , and the energy  $V(0) = E_0 = 0$  [continuous (green) horizontal line] defines the energy of a cusp-like homoclinic connection in the  $(w, w')$  phase-plane; it is depicted by the continuous (green) curve in the top-right panel (see also [21]). The corresponding analytical rational solutions  $R^r(x, t)$  and  $B^r(x, t)$  of the system are given by (45) and (46). The energy values  $E_0 < 0$  (dashed horizontal curves in the left-panel) are associated with the periodic orbits in the phase plane (dashed closed curves in the right-panel).

The spatial profiles of the coherent structure which is associated with the rational solution are illustrated in the bottom panels of Figure 11. The bottom-left panel shows the  $R^r(x, t)$  component at  $t = 0$ , and the bottom right

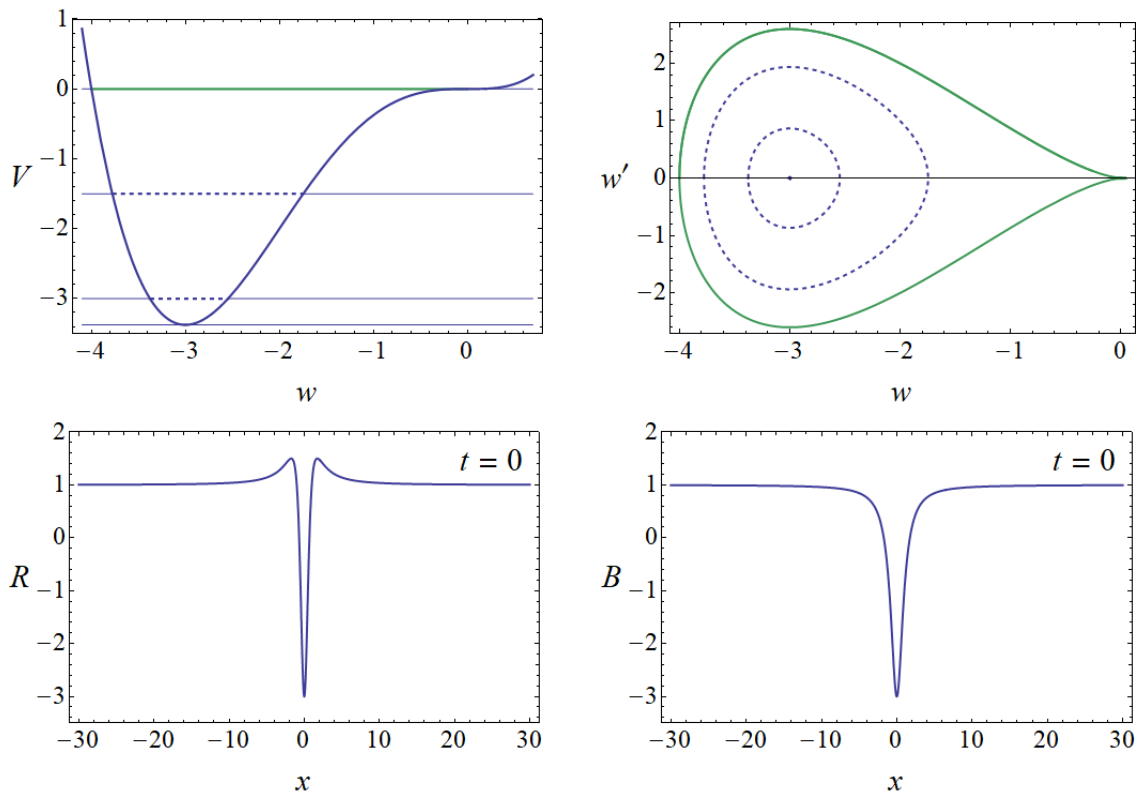


FIG. 11: Top-left panel: The graph of the effective potential when  $v = C$ , the case of the degenerate ODE Eq. (43). The (green) horizontal line defines the energy  $V(0) = E_0 = 0$  of the homoclinic connection associated with the analytical rational solutions (45)-(46). Top-right panel: The (green) continuous curve is the homoclinic connection of energy  $V(0) = E_0 = 0$ . The closed (dashed), periodic orbits correspond to energy values  $E_0 < 0$  (dashed horizontal lines in the left-panel). Bottom-left panel: The profile of the rational solution  $R^r(x, t)$ , given by Eq. (45), at  $t = 0$ . Bottom-right panel: The profile of the rational solution  $B^r(x, t)$ , given by Eq. (46), at  $t = 0$ .

panel shows the  $B^r(x, t)$ -component, at  $t = 0$ .

We have attempted to integrate the system with initial conditions  $R^r(x, 0)$  and  $B^r(x, 0)$ , but have found that the dynamics is extremely sensitive to small perturbations giving rise to numerical instabilities. We have noted also that the kind of numerical instability appearing is dependent on the choice of the half-length  $L$ . This is to be expected given the algebraic decay-rate of the initial conditions. Thus, even for a choice of  $L = 1000$  the initial error at the boundaries is of the order of  $\mathcal{O}(10^{-6})$  which can introduce numerical problems. In particular, considering these as small perturbations, the dynamical behavior of the solution turns out to be highly unstable.

This is a strong indication of the dynamical instability of this state. Thus, due also to its featuring negative density in part of the domain (hence being of rather limited physical relevance), we have not pursued it further.

#### IV. CONCLUSIONS

We studied the Adlam-Allen (AA) system of partial differential equations, one of the prototypical and fundamental models for the description of hydrodynamic disturbances in collisionless plasmas. The phase-plane analysis for the relevant, effective second order conservative dynamical system (associated with the description of traveling waves), enabled us to identify exact soliton solutions for the original system. In line with the original work of [1], we have found that these waves have velocities between once and twice that of the characteristic Alfvén speed.

Another important finding was the establishment of the strong connection of the Adlam-Allen system with the Korteweg-de Vries equation: we found that in the small-amplitude limit, the solitary waves of the original AA system transform into the soliton solutions of the Korteweg-de Vries equation. This connection was already highlighted, when studying the linearization of the Adlam-Allen system: we found that this can be described by a linearized improved Boussinesq equation, which, in the long wave approximation and in the weak dispersion regime, features the same

dispersion relation as the Korteweg-de Vries equation.

The above justifications motivated us to study by direct numerical simulations, not only the dynamics of the exact soliton solutions, but also the interaction dynamics of two soliton waveforms, initialized through a superposition of the analytical solitary waves. First, the stable evolution of individual exact pulses was observed in agreement with the analytical arguments for their derivation. In the more interesting case of soliton interactions, we examined two scenarios. In the first scenario where the velocity of the one soliton is close to the Alfvén speed, and the velocity of the second is considerably higher, we found a quasi-elastic collision: the fast soliton overtakes the slow-one, and both almost preserve their velocities and shape. The weak inelasticity of the collision was detected by the emission of small amplitude linear waves. The occurrence of the latter is further suggesting that the Adlam-Allen system might be non-integrable. In the second scenario, where both soliton velocities take values close to twice of the Alfvén speed, we observed an interaction of repulsive type; after an exchange of their velocities, the solitary waves continued their propagation in the same direction, emitting far weaker wavepackets (in comparison to the previous case).

The dynamical systems analysis verified also the existence of spatially periodic solutions. A numerical study examining the dynamics of such solutions in the presence of small perturbations, suggests that these spatially periodic travelling waves might be robust. Finally, the same dynamical analysis was used to reveal the existence of rational solutions, possessing an algebraic decaying rate in the limiting case of propagation at the Alfvén speed. It is worthwhile to note that such solutions are of growing interest due to their argued relevance within the context of rogue waves [18, 19]. While such solutions are not of physical interest here (since they feature negative densities in part of the spatial domain), they are certainly of interest from a mathematical point of view. Remarkably, they are associated with a degenerate case of the effective conservative dynamical system. Yet, they are unfortunately found to be quite unstable numerically.

This study is only a first step towards an attempted revival of the interest in the Adlam-Allen model. While we have explored special solutions and their full PDE dynamics, numerous questions remain unexplored. Among them, a predominant one is whether the model possesses a (presumed) Hamiltonian structure and what the corresponding conserved quantities may be. Additionally, from a mathematical analysis point of view, well-posedness properties (local and global) appear to us worthwhile to study, in analogy to the well-established counterpart of the KdV model. A more definitive view of the potential integrability of the problem (or, more likely, lack thereof) could be an interesting direction to pursue in its own right. Finally, we note that this model concerns the analysis of a transverse magnetic field, while recently [22], the longitudinal, far more complex case has also been considered. Expanding the lines of thinking of the present work regarding multiple solitary waves, and their interactions, as well as generalized periodic solutions is also of interest. Work along these directions is currently in progress and will be reported in future studies.

- 
- [1] J. H. Adlam and J. E. Allen, *Philosophical Magazine* **3**, 448–455 (1958).
  - [2] J. H. Adlam and J. E. Allen, *Proc. Phys. Soc.* **75**, 640 (1960).
  - [3] N. J. Zabusky and M. D. Kruskal, *Phys. Rev. Lett.* **15**, 240 (1965).
  - [4] E. Fermi, J. Pasta, and S. Ulam, *Tech. Rep. Los Alamos Nat. Lab. LA1940* (1955).
  - [5] D. J. Korteweg and G. de Vries, *Phil. Mag.* **39**, 422 (1895).
  - [6] H. Washimi and T. Taniuti, *Phys. Rev. Lett.* **17**, 996 (1966).
  - [7] E. Infeld and G. Rowlands, *Nonlinear Waves, Solitons and Chaos*, Cambridge University Press (Cambridge, 1990).
  - [8] M. Kono and M. M. Skorić, *Nonlinear Physics of Plasmas*, Springer-Verlag (Heidelberg 2010).
  - [9] J. E. Allen, *Phys. Scripta* **57**, 436 (1998).
  - [10] J. E. Allen, and J. Gibson, *Phys. Plasmas* **24**, 042106 (2017).
  - [11] M. J. Ablowitz, *Nonlinear Dispersive Waves: Asymptotic Analysis and Solitons* (Cambridge University Press, Cambridge, 2011).
  - [12] N. Meyer-Vernet, *Basics of the solar wind*, (Cambridge University Press, Cambridge, 2007).
  - [13] I. S. Gradshteyn, I.M. Ryzhik, *Table of Integrals, Series, and Products*, Academic Press (Cambridge, 1994).
  - [14] M. Remoissenet, *Waves Called Solitons* (Springer, Berlin, 1999).
  - [15] I. L. Bogolubsky, Some examples of inelastic soliton interactions, *Comp. Phys. Comm.* **13**, 149-155 (1977).
  - [16] A. Jeffrey and T. Kawahara, *Asymptotic Methods in Nonlinear Wave Theory* (Boston, MA, Pitman, 1982).
  - [17] W. E. Schiesser, *The numerical method of lines*, (Academic Press, 1991).
  - [18] C. Kharif, E. Pelinovsky, and A. Slunyaev, *Rogue Waves in the Ocean* (Springer, New York, 2009).
  - [19] M. Onorato, S. Residori and F. Baronio, *Rogue and Shock Waves in Nonlinear Dispersive Media* (Springer-Verlag, Heidelberg, 2016).
  - [20] N. Bottman, B. Deconinck, *Discr. Cont. Dyn. Sys. A* **25**, 1163 (2009).
  - [21] J. K. Hale and H. Koçak, *Dynamics and Bifurcations* (Springer-Verlag, New-York, 1991)
  - [22] G. Abbas, J.E. Allen, M. Coppins, L. Simons, L. James, *A study of the propagation of a solitary wave along the magnetic field in a cold collision-free plasma*, preprint (2019).